Magnetic edge states and coherent manipulation of molecular graphene nanoribbons

*Michael Slota,[1,2] Ashok Keerthi,[3] William K. Myers,[2] Evgeny Tretyakov,[4] Martin Baumgarten,[3] Arzhang Ardavan,[2,5] Hatef Sadeghi,[6] Colin J. Lambert,[6] Akimitsu Narita,[3] Klaus Müllen,[3] and Lapo Bogani[1,2]**

[1] Department of Materials, University of Oxford, 16 Parks Road, OX1 3PH, Oxford, United Kingdom.

[2] Centre for Advanced ESR, University of Oxford, South Parks Road, OX1 3QR, Oxford, United Kingdom.

[3] Max-Planck-Institut für Polymerforschung, Ackermannweg 10, 55128, Mainz, Germany.

[4] N. N. Vorozhtsov Novosibirsk Institute of Organic Chemistry, 9 Ac. Lavrentiev Avenue, Novosibirsk 630090, Russia.

[5] Clarendon Laboratory, University of Oxford, Parks Road, OX1 3PU, Oxford, United Kingdom.

[6] Quantum Technology Centre, Physics Department, Lancaster University, LA1 4YB, Lancaster, United Kingdom.

Keywords: graphene, graphene nanoribbons, molecular magnets, bottom-up synthesis.

Graphene, a single-layer network of carbon atoms, shows outstanding electrical and mechanical properties,[1] and graphene ribbons with nanometer-scale widths,[2,3] should exhibit half-metallicity,[4] quantum confinement and edge effects.[5,6] Magnetic edges in graphene nanoribbons have undergone intense theoretical scrutiny, because their coherent manipulation would be a milestone for spintronic[7] and quantum computing devices.[8] Experimental investigations are however hampered by the fact that most nanoribbons do not have the required atomic control of the edges, and that the proposed graphene terminations are chemically unstable[9]. Here we solve both of these problems, by using molecular graphene nanoribbons functionalized with stable spin-bearing radical groups. We observe the predicted delocalized magnetic edge states, and test present theoretical models about the spin dynamics and the spin-environment interactions. Comparison with a non-graphitized reference material allows clear identification of fingerprint behaviours. We quantify the spin-orbit coupling parameters, define the interaction patterns, and unravel the spin decoherence channels. Even without any optimization, the spin coherence time is in the μs range at room temperature, and we perform quantum inversion operations between edge and radical spins. This new approach to problem of spins in well-defined electronic nanostructures offers a long-awaited experimental testbed for the theory of magnetism in graphene nanoribbons. The observed coherence times open up encouraging perspectives for the use of magnetic nanoribbons in quantum spintronic devices.

Theory predicts that graphene nanoribbons (GNRs) can have magnetic edges,[6] which would display ferromagnetism and excellent spin filtering properties,[7] in addition to interesting quantum-coherence features.[8] On the other hand, most GNRs do not have atomically-precise edges and bare graphene terminations are very sensitive to chemical modification,[9] so that the properties of magnetic edge states, and even whether they exist at all, is still uncertain. Previous results using microscopy have largely been blind to the magnetic effects. We have developed the bottom-up molecular synthesis, allowing for the fabrication of atomically precise GNRs with various structures, which can be uniquely defined by the shape of molecular precursors.[10,11,10] We have very recently demonstrated the synthesis of pure zigzag GNRs showing localized edge states in ultra-high vacuum, but the magnetic characterizations turned out to be highly challenging due to their instability, so that the spin properties of such well-defined zigzag GNRs remain largely unexplored.[11,12]

We overcome these problems by injecting a spin density into the edge states of stable molecular GNRs synthetized via solution-based bottom-up chemical methods, using nitronyl-nitroxide radicals[13] (NIT) as magnetic injectors. The advantages of this approach are that: the magnetic functionalities are well known,[13] instead of relying on still-undefined magnetic states and they show interesting quantum properties;[14] the sample can be mass-produced, instead of appearing just on one device; and we can test the classical and quantum spin properties in depth; the systems are chemically very stable.

The synthesis of NIT-functionalized GNRs (NIT-GNRs) starts with Diels–Alder polymerization of a bromo-functionalized tetraphenylcyclopentadienone-based monomer **1**, yielding a bromo-substituted precursor polymer **2** (Fig.1a). Palladium-catalysed cross-coupling of **2** to triphenylphosphine-gold(I)-(nitronyl-nitroxide-2-ide) yields the magnetic NIT-polyphenylen**e**, which provides a non-graphitized reference material (Fig.1b). Graphitization of **2** yields the bromo-substituted nanoribbons **3**, which are magnetically functionalized to NIT-GNRs by partial bromine substitution via cross-coupling (Fig.1c).[15] Size-exclusion chromatography of **2** yields an average molecular weight of 126 kg/mol, corresponding to an average nanoribbon length $\bar{l} > 100$ nm. FTIR, Raman and UV-Vis spectroscopies corroborate the well-defined NIT-GNR structure, as in previous reports,[15] without appreciable presence of transition-metal magnetic impurities (SI).

The unpaired electron of the nitronyl-nitroxide resides in a π-orbital extending over two N–O groups and a C atom, which overlaps considerably with the π-orbitals of the aromatic backbone, and is known to inject spin into aromatic substituents (SI).[16] Modelling of NIT-GNRs using density functional theory shows a sizeable spin density injected into the graphene backbone, creating localized, non-dispersive states and magnetic dispersive edge state, while the spins of the NIT-polyphenylene remain in completely localized states (Fig.1b,c and SI).

We can directly observe and manipulate the spin states using electron spin resonance[17] (ESR), where the spin levels are split by a magnetic field and transitions are induced by microwave absorption. Static spectra at different frequencies (Fig.2a) are reproduced using the spin Hamiltonian:

1) $H = H_Z + H_{Hy} + H_D + H_{Ex}$,

where the Zeeman term $H_Z = \mu_B \boldsymbol{B}\boldsymbol{g}\boldsymbol{S_i}$ contains the effect of the magnetic field $\boldsymbol{B}$ on the i-th spin $\boldsymbol{S_i}$, via the Landé tensor $\boldsymbol{g}$; $H_{Hy} = \sum_{i,n} \boldsymbol{S_i}\boldsymbol{A_{in}}\boldsymbol{I_n}$ is the hyperfine interaction between the electron spin and the spin of the nucleus n; $H_D = \sum_{i \neq j} \boldsymbol{S_i}\boldsymbol{D_{ij}}\boldsymbol{S_j}$ is the dipolar coupling, with $D = g_i g_j \mu_0 \mu_B^2 \left(4\pi r_{ij}^3\right)^{-1} \mathrm{diag}(-1,-1,2)$, that contains the vacuum permeability μ_0, the Bohr magneton μ_B and the spin-spin distance r; $H_{Ex} = \sum_{i \neq j} J\boldsymbol{S_i}\boldsymbol{S_j}$ represents the exchange coupling. The parameters that best reproduce all frequencies are: $\boldsymbol{g}$=[2.0097(5), 2.0060(4), 2.0026(1)]; hyperfine coupling with the ^{14}N atoms $\boldsymbol{A_N}$=[0.0, 3(2), 34(2)] MHz, tilted by φ=9° in-plane relative to the $\boldsymbol{g}$ tensor; D_{12}=D_1=11.0±0.5 MHz and D_{13}=D_{23}=D_2=8.5±0.5 MHz for the along and across-edge interactions, respectively (Fig2b). Within error, the same results are obtained for the radicals on NIT-GNRs: $\boldsymbol{g}$=[2.0098(5), 2.0059(5), 2.0026(1)], $\boldsymbol{A_N}$=[0.0, 5(2), 34(2)], D_1=11.0±0.5 MHz, D_2=8.5±0.5 MHz. The inter and intra-edge exchange interactions are J_1=–25±5 MHz, J_2=12±3 MHz, in agreement with the sign expected from theoretical predictions[18] and Goodenough-Kanamori rules.[13] These signals are to be attributed to the spin density localized on the nitronyl-nitroxides.

In addition to this signal, NIT-GNRs display the predicted edge-state as an intense feature with uniaxial anisotropy: $g_{\|}$=2.0024(3), $g_{\perp}$=2.0041(2). Metallic impurities would produce ESR linewidths of tens of mT, vs the 1-2 mT observed. Metals and spin-bearing defects in the graphene backbone would have a different hyperfine coupling than the NITs, would not display all the characteristics of NIT radicals and the DEER experiments would not be possible with randomly-placed impurities (see later).

Its shape and linewidth rule out magnetic impurities and match previous hints of delocalized spin states,[19] providing the smoking gun for the existence of edge spin states, long predicted for graphene nanoribbons.[4-7] Theory predicts that the honeycomb lattice of graphene introduces an axial spin-orbit effect, Δ_{SO}, while the breaking of the mirror symmetry of the plane produces a Rashba-type transverse term, Δ_R, yielding the Hamiltonian $H_{SO} = \pm\Delta_{SO}\sigma_z S_z + \Delta_R(\pm\sigma_x S_x - \sigma_y S_y)$, where ± denote the valley degrees of freedom, S_i and σ_i spin and pseudospin Pauli matrices.[8] Δ_{SO}≈15 μeV and Δ_R≈1 μeV are extracted by considering that $|\Delta E(g_i - g_e)| = 2\Delta_i$, where g_e is the free electron value, and perturbation theory is used to account for the effect of excited states at energy ΔE (available from the *ab-initio* calculations). This constitutes a direct experimental confirmation of tight-binding estimates of spin-orbit coupling in graphene,[20,21] and its suppression compared to carbon nanotubes, predicted by the lattice symmetry and the absence of curvature.[5,21] These observations, together with the fact that the static spectra are largely

insensitive to exchange interactions, indicate that the NIT-GNRs fall into a very interesting regime, where coherent manipulation of the spins is possible.

We thus explore the quantum spin coherence using time-resolved ESR. The quantum evolution of a spin can be represented as a movement over the Bloch sphere, with zenithal positions pure $|1/2\rangle$ and $|-1/2\rangle$ states, and all their possible combinations mapped on the sphere (Fig.3a). The spin-relaxation-time, T_1, represents spin-flips (vertical displacement), while the phase-memory-time, T_2, describes the evolution of the quantum phase information (azimuthal movement). We measure T_1 via the picket-fence technique[22] and T_m (a measure of the dephasing time) by the Hahn-echo decay. We fit the echo-signal Y with an exponential function $Y(\tau) = Y_0 e^{-\left(\frac{2\tau}{T_m}\right)^x}[1 + k_1\sin(2\omega\tau + \varphi_1) + k_2\sin(4\omega\tau + \varphi_2)] + c$ that contains modulation by the environment at a frequency ω (amplitudes k_1 and k_2 for first- and second-order effects) and a stretch parameter x (Fig.3b). We always find x=1, indicating that the relaxation time approximation is good, successive events are uncorrelated, and $T_m \approx T_2$ as traditionally defined.[23]

The T_1 values, ~10^{-5} s, validate theoretical predictions by analytical methods.[24] The temperature-dependence of T_1^{-1} (Fig.3c) shows three main regimes: a linear one below 25 K, characteristic of spin-phonon energy transfers; a Raman region between 25 and 200 K, where relaxation happens via virtual states; a room-temperature region where local vibrational modes play a role, with the same characteristic energy (1354 cm^{-1}) for NIT-GNR and NIT-polyphenylene, tentatively assigned to the N–O stretching mode. Theories of low-temperature spin-phonon relaxation in graphene[5,20] quantum dots consider a deformation-potential-mechanism, active for longitudinal-acoustic phonons, and a bond-length-change mechanism, active for transversal- and longitudinal-acoustic modes. These, in conjunction with the absence of Van Vleck cancellation,[20] are predicted to generate the linear dependence indeed observed here, at low fields. The other hypothesized mechanism, spin-state-admixture,[5] can be ruled out by the observed temperature- and field-dependences and the low value of the observed Rashba spin-orbit-coupling, to which it is linked by symmetry selection rules.[5,20]

Even without any optimization, NIT-GNRs display T_m=0.5 μs at room-temperature and 1.1 μs at 85 K (Fig.3c and SI), 100 times longer than the 12 ns available in spintronic devices.[25] The high value is likely linked to the efficient suppression of scattering in atomically-regular edges. NIT-GNRs show only a slight increase of T_m at lower temperatures, while NIT-polyphenylene shows a minimum at 170 K and a broad maximum at 60 K, attributable to the progressive freezing of the benzene-benzene σ-bonds in the backbone. Although T_m for the localized radicals in NIT-polyphenylene might be slightly longer, the NIT-GNRs allow validating theories of spin relaxation in graphene, possess an edge-state that is connected to transport and is promising for quantum operations.

We now proceed to determine the sources of decoherence in NIT-GNRs. The modulation of the Hahn-echo amplitude (Fig.3b) at $\omega/2\pi$=3.6 MHz, a frequency typical of ^{13}C spin-nuclei interactions,

suggests that hyperfine decoherence channels are important. Electron-electron-double-resonance-detected-nuclear-magnetic-resonance, EDNMR, allows de-convoluting the different nuclear contributions[16,23] (Fig.4a). ^{14}N coupling is dominant, confirming the analysis of CW spectra, but ^{13}C, ^{1}H single-quantum-transitions, ^{14}N, ^{13}C double-quantum-transitions and nitrogen-carbon mixed-transitions also play an important role. The coupling strength to the ^{13}C of the graphene backbone ~10MHz, is considerably smaller than theoretical estimates for confined graphene dots,[5,26] where anisotropic, Fermi-contact and nucleus-orbital interactions contribute to a total ^{13}C hyperfine interaction of ~70 MHz. These couplings suggests that nuclei could be used as computational resources.[27]

We eventually consider the coupling between localized spins and the edge state. Information about electron-electron interactions is obtained by four-pulse double-electron-electron-resonance (DEER, Fig.4b),[17,22] where the system is initialised and probed at the g_x resonance of the radicals, and perturbed at the resonance condition of the edge-state. The resulting spectrum displays an intriguing slow oscillation that is overlaid with fast ones (Fig.4c). The fast period corresponds to the D_1 and D_2 interactions, which are too strong for accurate resolution using DEER, and are better appreciated via the CW spectra. Slow oscillations correspond to interactions between localized and edge-state spin yielding a radical-edge spin interaction of 1.5 MHz (Fig.4d); these oscillations are absent in NIT-polyphenylene, in agreement with the lack of edge-states. The extracted edge-radical spin-inversion time, ~330 ns, is considerably shorter than T_m, enabling coherent inversion operations using graphene edge-states and localized spins. This, in conjunction with recent results on the transport on molecular nanoribbons, opens fascinating possibilities: quantum operations can in principle be performed via single-electron transport, and the spin states detected electrically, so that our radical-substituted NIT-GNRs seem ideal candidates for quantum nanoelectronic devices. The interaction of multiple radical spins with a coherent, delocalized edge-state, could allow a single flowing electron to transmit entanglement along the spin ensemble.[8] Furthermore, such molecular nanoribbons are a useful testbed for fundamental theories of graphene, and our measurements of spin-orbit, hyperfine and edge-spin coupling already disclose a physics that would otherwise be accessible only by overcoming present challenges in quantum-Hall-effect studies at sub-mK temperatures.[20,21] Detailed access to the spin dynamics, together with an atomically-defined structure, opens the path to the quantitative analysis of spin-phonon interactions in graphene dots. The study of different molecular spin-injectors and of different aromatic backbones,[10] e.g. to modulate the spin coupling, opens up a new area of chemistry that mixes molecular magnetism and graphene. Environmental effects, such as GNR-GNR or GNR-substrate interactions are an interesting future area of research and calculations show, encouragingly, no detrimental effect on the spin density by deposition on h-BN (SI). With respect to applications, since a dominant decoherence channel is ^{14}N hyperfine coupling, there is ample room to increase T_2, e.g. by, dynamic nuclear spin polarization[28], isotopic substitution[29] or chemical engineering[30]. Full investigations of magnetic doping effects and of incomplete edge

functionalization with radicals is currently underway, and will introduce graphene nanoribbons as a powerful tool to investigate finite-size-effects in quantum Heisenberg spin-chains.[18]

Methods

Precursors. All chemicals were used as purchased without further purification. All reactions dealing with air- or moisture-sensitive compounds were carried out in a dry reaction vessel under argon. The starting materials S1, Poly-Br and GNR-Br were synthesised adapting published protocols[31] and the detailed synthesis is reported in the supplementary information. Unless otherwise noted, materials were purchased from commercial suppliers (Fluka, Aldrich, Acros, ABCR, Merck and other) and used as received without further purification unless otherwise specified.

Material Characterization. Analytical size exclusion chromatography (SEC) was performed on SDV PSS GPC columns using THF as eluent at a temperature of 303 K. Absorbance was determined on a UV S-3702 detector (SOMA) at a fixed wavelength of 270 nm. The samples were referenced with respect to standard polystyrene (PS) as well as poly(p-phenylene) (PPP) calibration curves. Solution UV–vis absorption spectra were recorded at room temperature on a Perkin-Elmer Lambda 900 spectrophotometer. GNR samples were dispersed in N-methyl-pyrrolidone (NMP) by using sonication (30 min) in a Branson-1510 ultrasonicator followed by filtration through 5 micron Polytetrafluoroethylene (PTFE) filters. Infrared spectroscopy was measured on a Nicolet 730 FT-IR spectrometer equipped with an attenuated total reflection (ATR) setup. The samples were deposited as pristine material on the diamond crystal and pressed on it with a stamp. Measurements with a scan number of 128 were recorded for each sample and the background was subtracted.

ESR spectroscopy. X-band (~9.5 GHz) and W-band (~94 GHz) ESR spectra were acquired using a Bruker EleXsys E680. Q-band ESR spectra were obtained on a Bruker EleXsys E580. X-band CW spectra were additionally recorded on a Bruker EMX. Sample temperature was maintained with an Oxford Instruments CF9350 cryostat, and controlled with an Oxford Instrument ITC503. Microwave resonators were Bruker ER4118X-MS-3W1 for X-band (Bruker E680), Bruker EN510702 for Q-band and Bruker EN600-1021H for W-band. The sample was prepared as lose powder in low-background quartz glass tubes. X-band CW measurements were calibrated using polystyrene. High-field measurements at Q-band and W-band frequencies were calibrated using a MgO standard. ***Continuous-wave ESR.*** CW measurements were performed at X-band and Q-band frequencies at room temperature. The modulation amplitude was set to 1 G and the modulation frequency to 100 kHz for X-band, and to 50 kHz for Q-band measurements. Spectra were simulated using the Matlab package EasySpin[32]. ***FID-***

detected ESR. FID(free-induction-decay)-detected ESR spectra at W-band frequency were obtained by excitation of the spin system with a long π-pulse. This allows detectable free induction decay signals (FID) to persist after the receiver protection switch. By integrating the signal against the field, the result comes very close to the integral of the corresponding CW-ESR experiment[33]. The measurement was performed at 85 K to ensure a strong signal. Spectra were simulated using the Matlab package EasySpin[32]. ***Determination of T_1.*** In the picket-fence pulse sequence (Fig. 3b), which we used to determine the spin-lattice relaxation time T_1, we set the π/2 and π pulse duration to 16 ns and 32 ns, respectively, and used a 4-step phase cycling procedure. The resulting data were fitted with a sum of two exponential functions, where one accounts for spin-lattice relaxation and the other one for spectral diffusion processes. Spectral diffusion arises from electron-electron and electron-nuclear couplings, thus adding another relaxation mechanism. The picket-fence pulse sequence minimises this contribution. ***Fit of T_1.*** We describe the spin-lattice relaxation by three main mechanisms, which scale differently with temperature. By considering direct relaxation, Raman processes and the excitation of local vibrational modes, we arrive at[34]:

$$\frac{1}{T_1} = A_{\mathrm{lin}}T + A_{\mathrm{Ram}}\left(\frac{T}{\theta_D}\right)^9 \int_0^{\frac{\theta_D}{T}} \frac{x^8 e^x \mathrm{dx}}{(e^x-1)^2} + A_{\mathrm{loc}}\left(\frac{e^{\Delta_{\mathrm{loc}}/T}}{\left(e^{\Delta_{\mathrm{loc}}/T}-1\right)^2}\right),$$

where A_{lin}, A_{Ram}, A_{loc} denote the rate constants of the three processes, θ_{D} is the Debye-temperature, x is an integration variable and Δ_{loc} is the excitation energy of a local vibrational mode. For both compounds we find θ_{D}=200 K, A_{loc}=3.5·10^7 s^{-1} and Δ_{loc}=1950 K (1354 cm^{-1}), in perfect agreement with the local excitation of the stretching modes of the N-O bond, as obtained by infrared spectroscopy[35]. Furthermore, we find A_{lin}=12 s^{-1}, A_{Ram}=3.0·10^{-16} s^{-1} for NIT-polyphenylene, and A_{lin}=55 s^{-1}, A_{Ram}=2.2·10^{-16} s^{-1} for NIT-GNR. Moreover, we note that the relaxation is affected by electron-electron interaction effects, as our samples are highly spin-concentrated. This results in a linear region even above 10 K, which is not related to direct relaxation[34]. ***Hahn-echo.*** The Hahn-echo sequence (Fig. 3b) enables the determination of the phase-memory time T_m, which represents an upper limit for T_2, as several effects such as instantaneous or spectral diffusion affect the measurement. We set the pulse durations to 16 ns for the π /2 pulse and 32 ns for the π pulse, phased the signal and integrated over the second half of the echo. We used a 16-step phase cycling procedure. We identified T_m to be equal to T_2. ***EDNMR spectroscopy.*** EDNMR (electron-electron double resonance nuclear magnetic resonance) was performed at Q-band frequency and at 85 K. Pulse shapes were formed using an arbitrary waveform generator. The Gaussian-shaped excitation pulse duration was set to 1200 ns, which allows for the excitation of forbidden nuclear transitions[36]. The detection π-pulse after a delay of t was set to 400 ns, and the FID was recorded. The central line around Δν = 0 was removed with Voigtian and additional Lorentzian lineshapes. ***DEER spectroscopy.*** DEER (double electron-electron resonance) measurements were performed at Q-band frequency and at 85 K. Pulses were created using the arbitrary waveform generator The durations of the detection pulses were set

to 12 ns and 18 ns for NIT-GNRs and NIT-polyphenylenes, respectively. The pump pulse (ELDOR pulse) duration was set to 20 ns. We integrated over the resulting echo against the variable time-delay of the ELDOR pulse. The shown time-domain DEER data was obtained after normalisation, long-pass filtering (23.5 MHz threshold) and subtraction of a three-dimensional background using the Matlab package DeerAnalysis[37].

Numerical calculations. Theoretical modelling was performed using the Gaussian[38] and SIESTA[39] implementations of density functional theory (DFT). For the spin density calculations of two systems shown in Fig. 1, Gaussian was used with a ulsda/6-311++g(d,p) functional and basis set and XQC method for the self-consistent reaction field. We found similar spin density using SIESTA. The generalized gradient approximation (GGA) of the exchange and correlation functional is used with the Perdew–Burke–Ernzerhof parameterization, a double-ζ basis set, a real-space grid defined with an equivalent energy cutoff of 150 Ry and a force tolerance smaller than 10 meV/Å. For the band structure calculation, each structure was sampled by a 1 × 1 × 15 Monkhorst–Pack k-point grid. We found the stable magnetic state by allowing the system to be spin polarized. Apart from the two edge atoms on the peripheral NIT 5-fold rings, atoms were numbered such that odd-numbered atoms are connected to even-numbered atoms only and vice versa. We then performed geometry optimisation of each system by choosing the initial system to have a ferromagnetic configuration (all spin up) or antiferromagnetic one where the odd (even) atoms are designated spin up (spin down). The total energy per unit cell of the antiferro-magnetically-aligned NIT-GNRs (NIT-polyphenylene) is 272meV (651meV) lower than ferro-magnetically-aligned one. The molecular orbitals, band structure and local density of state LDOS calculations were obtained using the anti-ferromagnetic spin alignment.

Data Availability Statement

The datasets generated during and/or analysed during the current study are available from the corresponding author on reasonable requ

Acknowledgments

We thank the European Research Council (ERC-StG 338258 OptoQMol), the EU (COST-CA15128, MOLESCO-606728 and Graphene Flagship), EPSRC (QuEEN grant), the Royal Society (University Research Fellowship and URF grant), RFBR (17-53-50043), the Max Planck Society and German DAAD Bilateral Exchange of Academics (2015/50015739) for financial support.

Author contributions

M.S. and W.M. performed the ESR characterization. A.K. and E.T. performed the synthesis and related characterization, for which M.B., A.N and K.M. provided supervision. H.S. and C.J.L. performed the

numerical modelling. M.S., W.M, A.A. and L.B. contributed to the ESR data analysis. M.S., A.N., K.M. and L.B. conceived the experiments and M.S. and L.B. wrote the manuscript. All authors contributed to the discussion and to the final version of the manuscript.

Author Information

Reprints and permissions information is available at www.nature.com/reprints. The authors declare no competing financial interests. Correspondence and requests for materials should be addressed to lapo.bogani@materials.ox.ac.uk .

Additional information

The authors declare no competing financial interests. Supplementary information accompanies this paper.

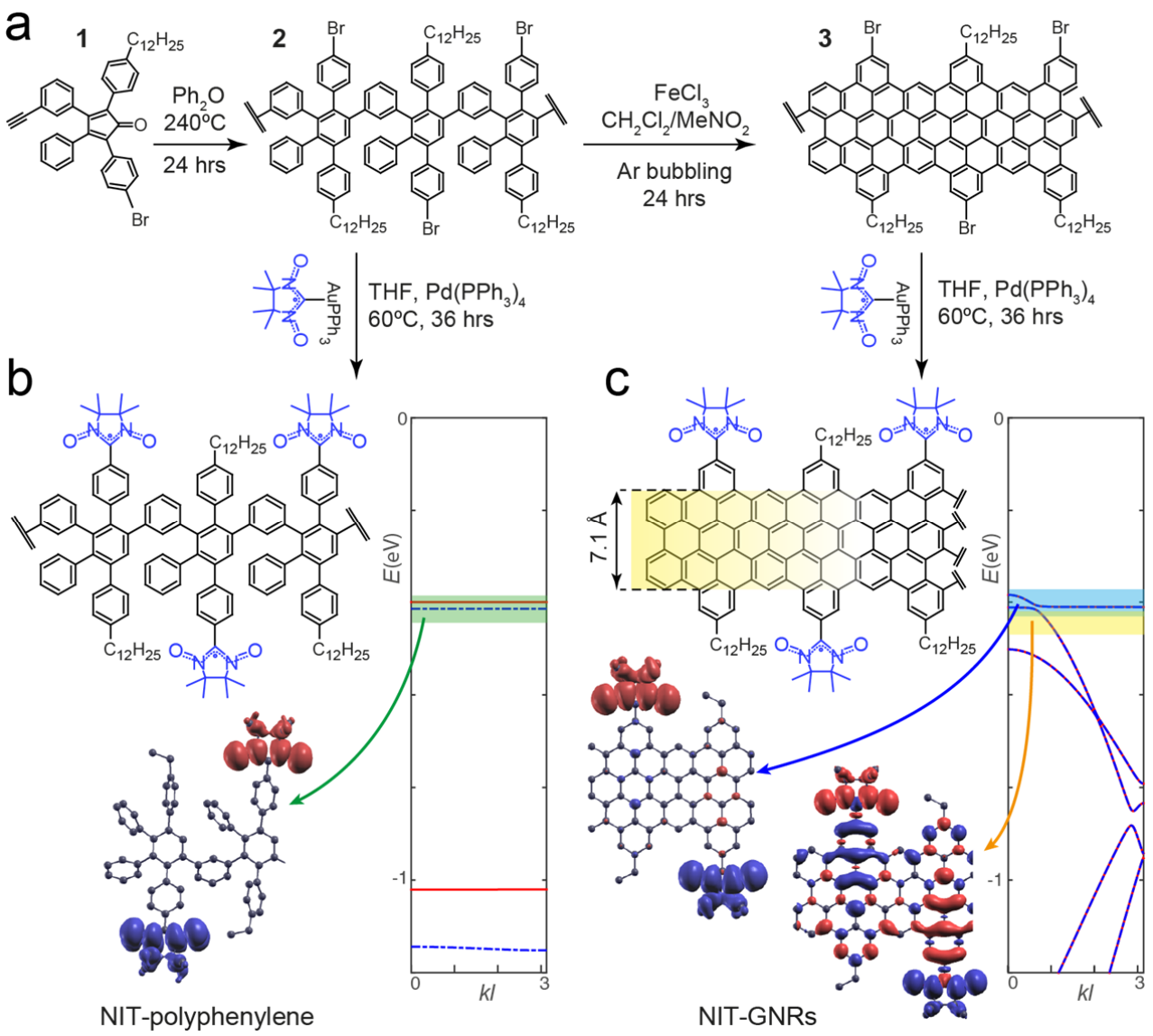

Figure 1. Functionalized graphene nanoribbons: a) Synthetic path to NIT-polyphenylene and NIT-GNRs, with spin-bearing radicals in blue. b) NIT-polyphenylene and its calculated local density of states. The energy levels (vs the wavevector *k* times the repeating unit length *l*) show no band structure and spins localized on the NIT groups. c) NIT-GNRs and its band structure, showing localized states and spin injection inside delocalized edge states. Densities calculated for different energy ranges are depicted (azure and orange shaded areas and arrows), with blue and red referring to local densities of spin up and down states, for a given energy interval.

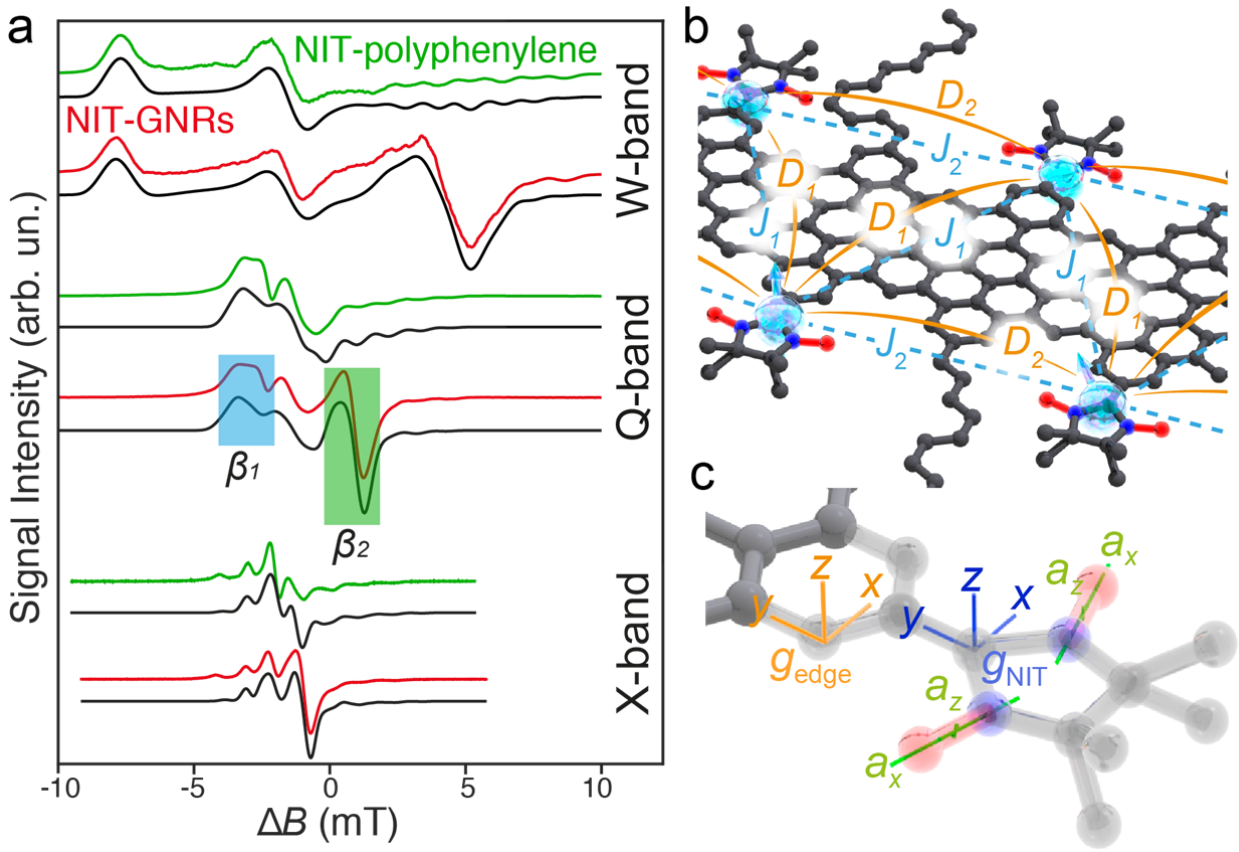

Figure 2. Static spectra and magnetic interaction pathways. a) Multi-frequency ESR spectra for NIT-polyphenylene (green) and NIT-GNRs (red) and simulations (black), plotted against the magnetic field from the edge-state resonance. DEER pump and probe windows are highlighted. b) Interaction pathways for radical spins, showing exchange (J_1 and J_2) and dipolar (D_1 and D_2) interactions. c) Orientation of the ^{14}N hyperfine channel (green), with the lengths of the axes proportional to the principal tensor elements (a_y smaller than the axis width) and orientations of the local ***g*** tensor frame of the radical (blue) and that of the graphene edge state (orange).

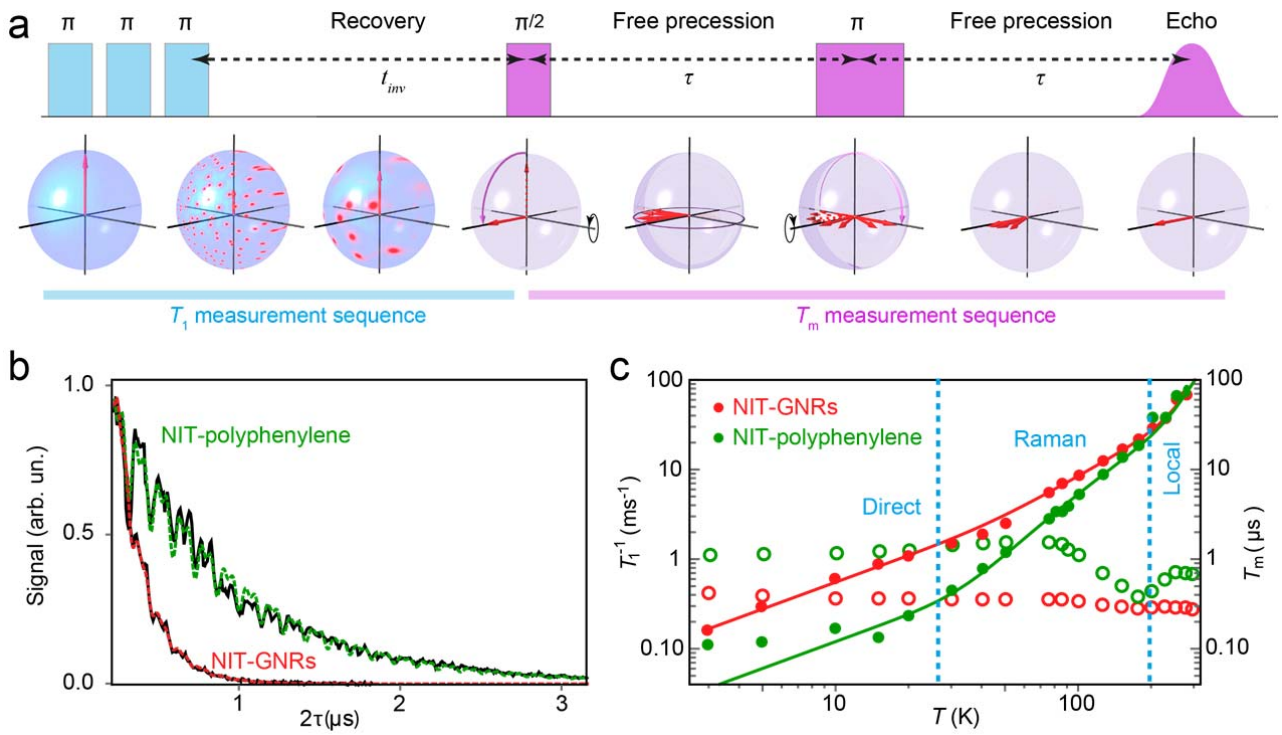

Figure 3. Spin-lattice and coherence times. a) Pulse sequence used to extract the spin relaxation times, and Bloch-sphere representation. A picket-fence series of π-pulses (azure) erases the spin polarization (red arrow), which recovers after a time T_1. The spins are then rotated to the xy-plane with a π/2-pulse (violet) and let free to precess for a time τ. A π-rotation in the middle of the free precession causes an echo signal when the spins regroup (red bell). b) X-band Hahn-echo signal *vs* delay time τ for NIT-GNRs and NIT-polyphenylene, at 85 K. Red and green lines are fits to the data, yielding T_m. c) T_1^{-1} (full dots, left axis) and T_m (open dots, right axis) vs temperature for NIT-GNRs (red) and NIT-polyphenylene (green), at 9.4 GHz. Lines are simulations for T_1^{-1} (see text), the dashed lines separate the different regimes of spin-lattice relaxation.

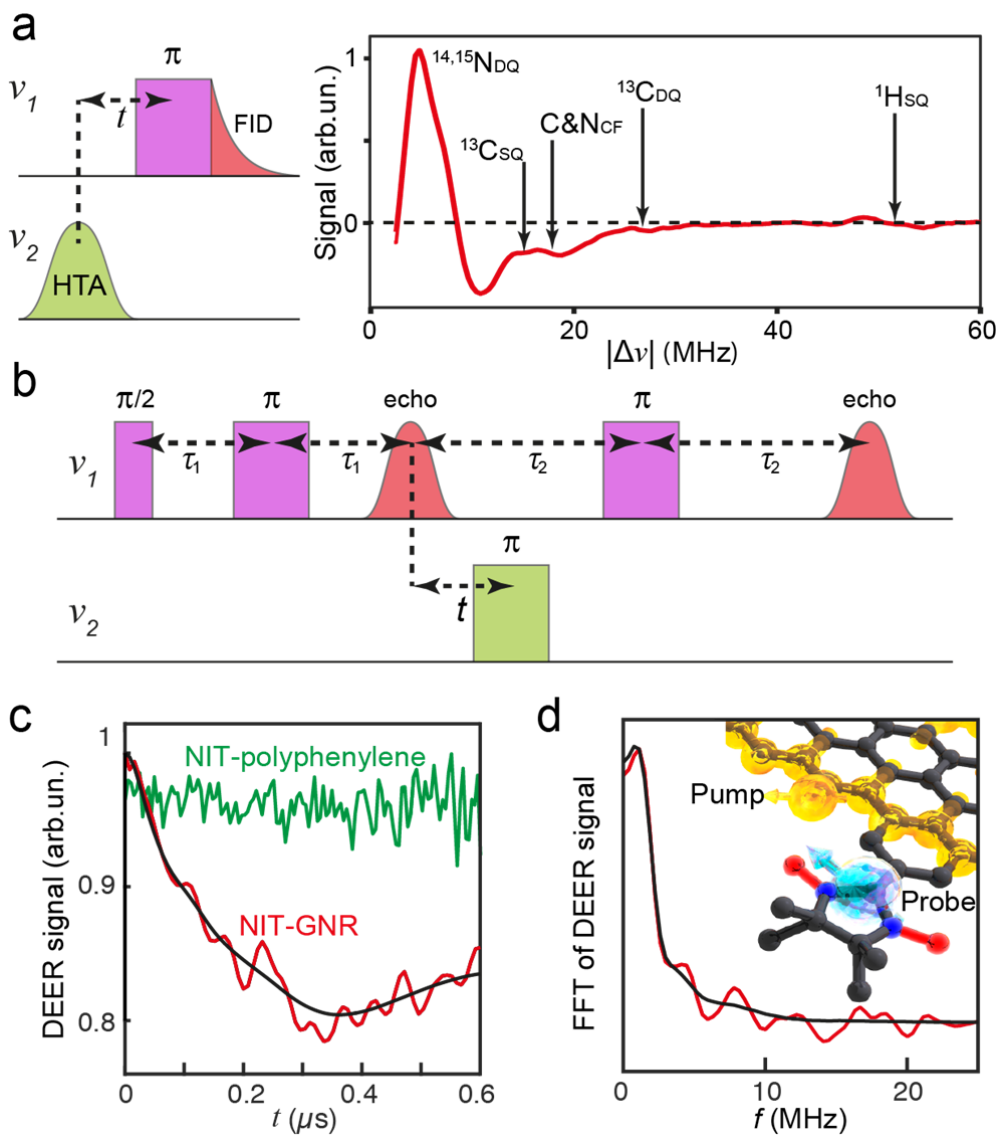

Figure 4. Hyperfine coupling and multi-spin operability in nanoribbons. a) Double-electron-electron-detected-nuclear-magnetic-resonance (EDNMR) sequence, using a high-turning-angle (HTA) pulse at ν_2, i.e. the edge-state-resonance β_2 (Fig.2a), while ν_1 is swept. The NIT-GNRs spectrum (Q-band, 85 K) shows single-quantum (SQ), double-quantum (DQ) and combination-frequency (CF) transitions. b) Double-electron-electron-resonance (DEER) sequence, with ν_1 set at the localized spin resonance and ν_2 at the edge state (β_1 and β_2 in Fig.2a), used to determine the spin-spin interactions and perform edge-local spin quantum inversion operations. c) Background-corrected time-domain DEER spectrum for NIT-polyphenylene (green) and NIT-GNRs (red). The black line singles out the low-frequency interactions. d) Fast Fourier transform (FFT) of the DEER signal of NIT-GNRs, showing the interaction energy spectrum characteristic of two-spin operations. The black line singles out the contribution from edges interacting with localized spins (drawing).

332 ***Bibliography:***

[1] Castro Neto, A. H., Guinea, F., Peres, N. M. R., Novoselov, K. S. & Geim, A. K. The electronic properties of graphene. *Rev. Mod. Phys*. **81**, 109 (2009).

[2] Jiao, L., Zhang, L., Wang, X., Diankov, G., & Dai, H. Narrow graphene nanoribbons from carbon nanotubes. *Nature* **458**, 877-880 (2009).

[3] Jia, X., Hofmann, M., Meunier, V., Sumpter, B.G., Campos-Delgado, J., Romo-Herrera, J.M., Son, H., Hsieh, Y.P., Reina, A., Kong, J. and Terrones, M. Controlled formation of sharp zigzag and armchair edges in graphitic nanoribbons. *Science*, **323**, 701-1705 (2009).

[4] Son, Y. W., Cohen, M. L., & Louie, S. G. Half-metallic graphene nanoribbons. *Nature* **444**, 347-349 (2006).

[5] Recher, P., & Trauzettel, B. Quantum dots and spin qubits in graphene. *Nanotechnology*, **21**, 302001(2010). And references therein.

[6] Meunier, V., Souza Filho, A. G., Barros, E. B., & Dresselhaus, M. S. Physical properties of low-dimensional sp_2-based carbon nanostructures. *Review of Modern Physics* **88**, 025005 (2016).

[7] Pesin, D., & MacDonald, A. H. Spintronics and pseudospintronics in graphene and topological insulators. *Nature Materials* **11**, 409-416 (2012).

[8] Trauzettel, B., Bulaev, D. V., Loss, D., & Burkard, G. Spin qubits in graphene quantum dots. *Nature Physics* **3**, 192-196 (2007)

[9] Barone, V., Hod, O., & Scuseria, G. E. Electronic structure and stability of semiconducting graphene nanoribbons. *Nano letters* **6**, 2748-2754 (2006).

[10] Narita, A., Wang, X.-Y., Feng, X. & Müllen, K. New advances in nanographene chemistry *Chem. Soc. Rev.* **44**, 6616-6643 (2015).

[11] Ruffieux, P., Wang, S., Yang, B., Sánchez-Sánchez, C., Liu, J., Dienel, T., Talirz, L., Shinde, P., Pignedoli, C. A., Passerone, D., Dumslaff, T., Feng, X., Müllen, K., & Fasel, R. On-surface synthesis of graphene nanoribbons with zigzag edge topology. *Nature* **531**, 489-492 (2016).

[12] Cai, J., Ruffieux, P., Jaafar, R., Bieri, M., Braun, T., Blankenburg, S., Muoth, M., Seitsonen, A.P., Saleh, M., Feng, X. & Müllen, K. Atomically precise bottom-up fabrication of graphene nanoribbons. *Nature* ***466***, 470-473 (2010).

[13] Caneschi, A., Gatteschi, D. & Rey, P. The Chemistry and Magnetic Properties of Metal Nitronyl Nitroxide Complexes. *Progress in Inorganic Chemistry* **39**, 331 (1991).

[14] Collauto, A., Mannini, M., Sorace, L., Barbon, A., Brustolon, M., & Gatteschi, D. A slow relaxing species for molecular spin devices: EPR characterization of static and dynamic magnetic properties of a nitronyl nitroxide radical. *Journal of Materials Chemistry* **22**, 22272-22281 (2012).

[15] Narita, A., Feng, X., Hernandez, Y., Jensen, S.A., Bonn, M., Yang, H., Verzhbitskiy, I.A., Casiraghi, C., Hansen, M.R., Koch, A.H., Fytas, G., Ivasenko, O., Li, B., Mali, K.S., Balandina, T., Mahesh, S., De Feyter, S. & Müllen, K. Synthesis of structurally well-defined and liquid-phase-processable graphene nanoribbons. *Nature Chemistry* **6**, 126-132 (2014).

[16] Zheludev, A., Barone, V., Bonnet, M., Delley, B., Grand, A., Ressouche, E., Rey, P., Subra, R. & Schweizer, J. Spin-density in a nitronyl nitroxide free-radical-polarized neutron-diffraction investigation and ab-initio calculations. *Journal of the American Chemical Society*, **116**, 2019 (1994).

[17] Schweiger, A., & Jeschke, G. *Principles of pulse electron paramagnetic resonance*. Oxford University Press, Oxford, UK (2001).

[18] Golor, M., Wessel, S., & Schmidt, M. J. Quantum nature of edge magnetism in graphene. *Physical review letters* **112**, 046601 (2014).

[19] Rao, S.S., Stesmans, A., van Tol, J., Kosynkin, D.V., Higginbotham-Duque, A., Lu, W., Sinitskii, A. & Tour, J.M. Spin dynamics and relaxation in graphene nanoribbons: electron spin resonance probing. *ACS nano* **6**, 7615-7623 (2012).

[20] Min, H., Hill, J. E., Sinitsyn, N. A., Sahu, B. R., Kleinman, L., & MacDonald, A. H. Intrinsic and Rashba spin-orbit interactions in graphene sheets. *Physical Review B* **74**, 165310 (2006).

[21] Kane, C. L. & Mele, E. J. Z_2 Topological Order and the Quantum Spin Hall Effect. *Physical Review Letters* **95**, 146802 (2005).

[22] Eaton, G. R. & Eaton, S. S. Multifrequency Electron Spin-Relaxation Times. *Multifrequency Electron Paramagnetic Resonance: Theory and Applications* (Ed. Misra, S. K., Wiley-VCH Verlag GmbH & Co. KGaA, Weinheim, Germany, 2011).

[23] Klauder, J. R. & Anderson, P. W. Spectral diffusion decay in spin resonance experiments. *Physical Review* **125**, 912 (1962).

[24] Struck, P. R. & Burkard, G. Effective time-reversal symmetry breaking in the spin relaxation in a graphene quantum dot. *Phys. Rev. B* **82**, 125401 (2010).

[25] Drögeler, M., Franzen, C., Volmer, F., Pohlmann, T., Banszerus, L., Wolter, M., Watanabe, K., Taniguchi, T., Stampfer, C. & Beschoten, B. Spin lifetimes exceeding 12 ns in graphene nonlocal spin valve devices. *Nano Letters* **16**, 3533 (2016).

[26] Fisher, J., Trauzettel, B. & Loss, D. Hyperfine interaction and electron-spin decoherence in graphene and carbon nanotube quantum dots. *Physical Review B* **80**, 155401 (2009).

[27] Dutt, M.G., Childress, L., Jiang, L., Togan, E., Maze, J., Jelezko, F., Zibrov, A.S., Hemmer, P.R. & Lukin, M.D., Quantum register based on individual electronic and nuclear spin qubits in diamond. *Science* **316**, 1312-1316 (2007).

[28] Foletti, S., Bluhm, H., Mahalu, D., Umansky, V. & Yacoby, A. Universal quantum control of two-electron spin quantum bits using dynamic nuclear polarization. *Nature Physics* **5**, 903-908 (2009).

[29] Balasubramanian, G., Neumann, P., Twitchen, D., Markham, M., Kolesov, R., Mizuochi, N., Isoya, J., Achard, J., Beck, J., Tissler, J., Jacques, V., hemmer, P.R., Jelezko, F. & Wrachtrup, J. Ultralong spin coherence time in isotopically engineered diamond. *Nature Materials* **8**, 383-387 (2009).

[30] Shiddiq, M., Komijani, D., Duan, Y., Gaita-Ariño, A., Coronado, E. and Hill, S. Enhancing coherence in molecular spin qubits via atomic clock transitions. *Nature* **531**, 348-351(2016).

Bibliography for Methods Section

[31] a) A. Narita, X. Feng, Y. Hernandez, S. A. Jensen, M. Bonn, H. Yang, I. A. Verzhbitskiy, C. Casiraghi, M. R. Hansen, A. H. R. Koch, G. Fytas, O. Ivasenko, B. Li, K. S. Mali, T. Balandina, S. Mahesh, S. De Feyter and K. Müllen, *Nat. Chem.* **6**, 126-132 (2014); b) A. Narita, I. A. Verzhbitskiy, W. Frederickx, K. S. Mali, S. A. Jensen, M. R. Hansen, M. Bonn, S. De Feyter, C. Casiraghi, X. Feng and K. Müllen, *ACS Nano* **8**, 11622-11630 (2014); c) A. Keerthi, I. C. Hou, T. Marszalek, W. Pisula, M. Baumgarten and A. Narita, *Chem. Asian J.* **11**, 2710-2714 (2016)

[32] S. Stoll and A. Schweiger, *J. of Magn. Reson.* **178(1)**, 42 (2006)

[33] T. Wacker, G. A. Sierra and A. Schweiger, *Isr. J. Chem.* **32**, 305-322 (1992)

[34] G. R. Eaton and S. S. Eaton, Multifrequency Electron Spin-Relaxation Times, in Multifrequency Electron Paramagnetic Resonance: Theory and Applications (ed S. K. Misra), Wiley-VCH Verlag GmbH & Co. KGaA, Weinheim, Germany (2011)

[35] L. Rintoul, A. S. Micallef and S. E. Bottle, *Spectrochim. Acta Part A* **70**, 713-717 (2008)

[36] N. Cox, W. Lubitz and A. Savitzky, *Mol. Phys.* **111**, 2788-2808 (2013)

[37] G. Jeschke, V. Chechik, P. Ionita, A. Godt, H. Zimmermann, J. Banham, C. R. Timmel, D. Hilger and H. Jung, *Appl. Magn. Reson.* **30**, 473 (2006)

[38] Gaussian 09, Revision A.02, Gaussian, Inc., Wallingford CT (2016)

[39] J. M. Soler, E. Artacho, J. D. Gale, A. García, J. Junquera, P. Ordejón and D. Sánchez-Portal, *J. Phys.: Condens. Matter* **14**, 2745 (2002)

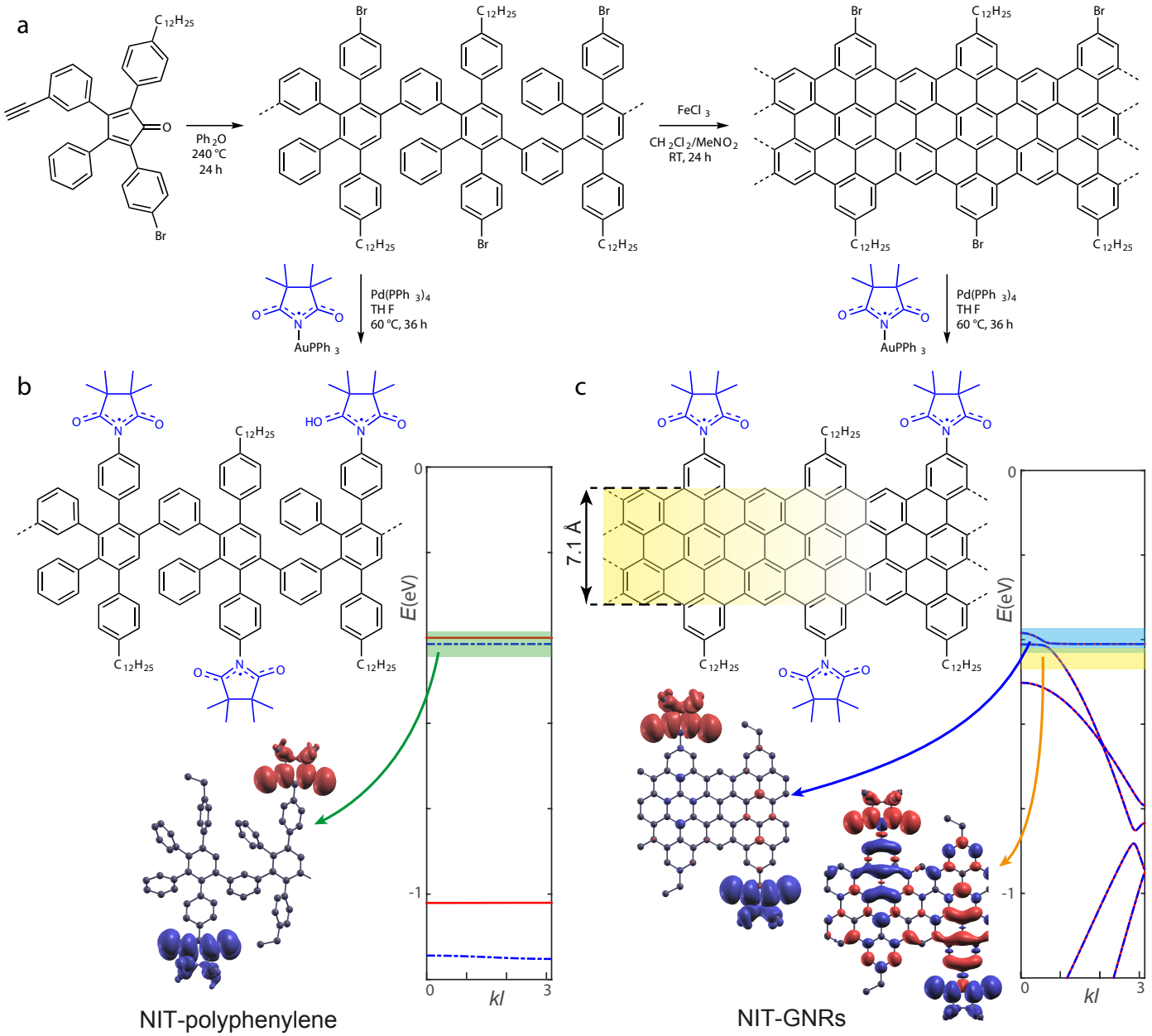
a
Ph2O
240 °C
24 h
FeCl3
CH2Cl2/MeNO2
RT, 24 h
Pd(PPh3)4
THF
60 °C, 36 h
AuPPh3
b
c
7.1 Å
E(eV)
kl
NIT-polyphenylene
NIT-GNRs

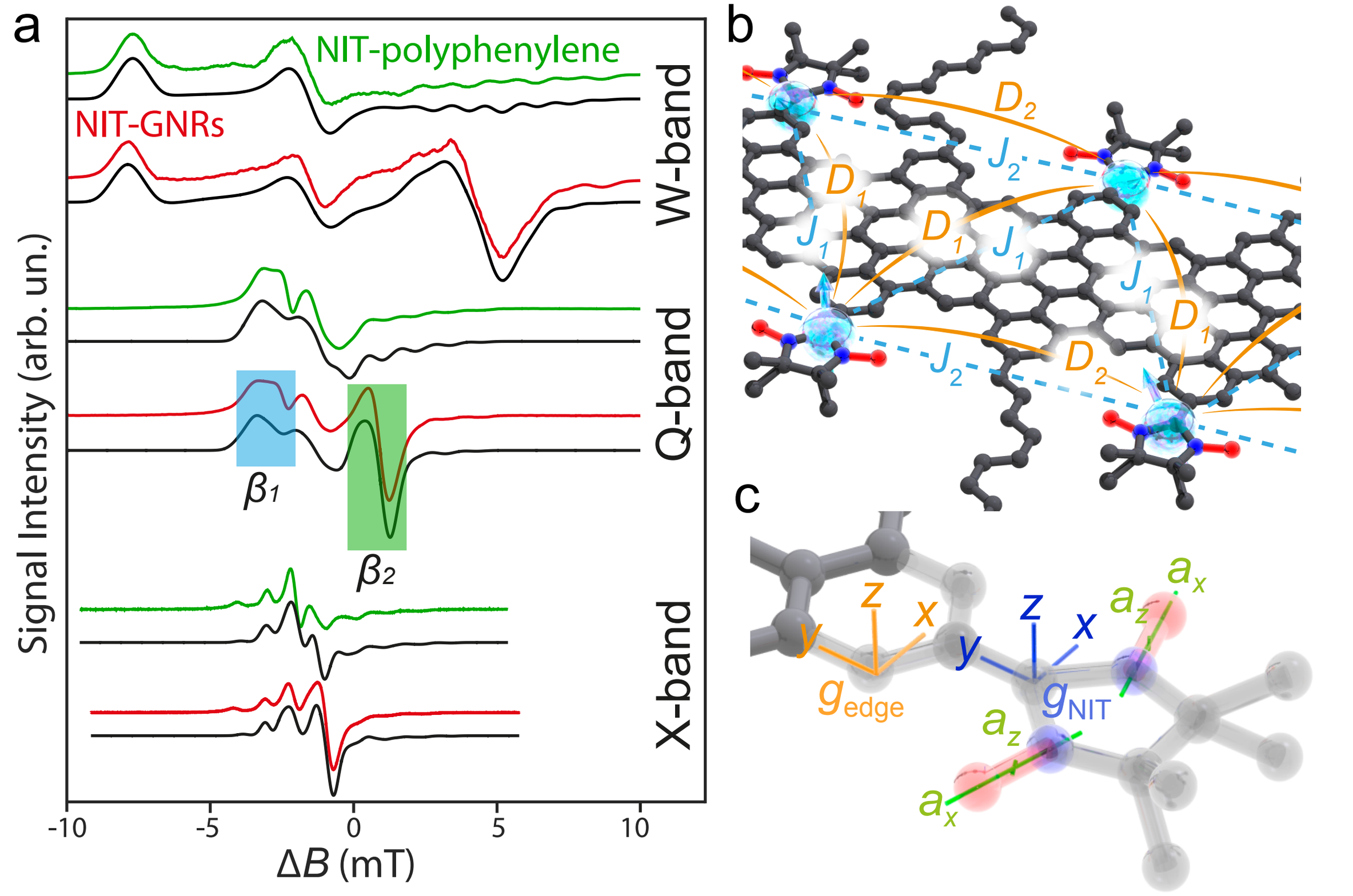
a
NIT-polyphenylene
NIT-GNRs
W-band
Q-band
X-band
β1
β2
Signal Intensity (arb. un.)
-10
-5
0
5
10
ΔB (mT)
b
D2
J2
D1
J1
c
z
x
y
gedge
gNIT
ax
az

a

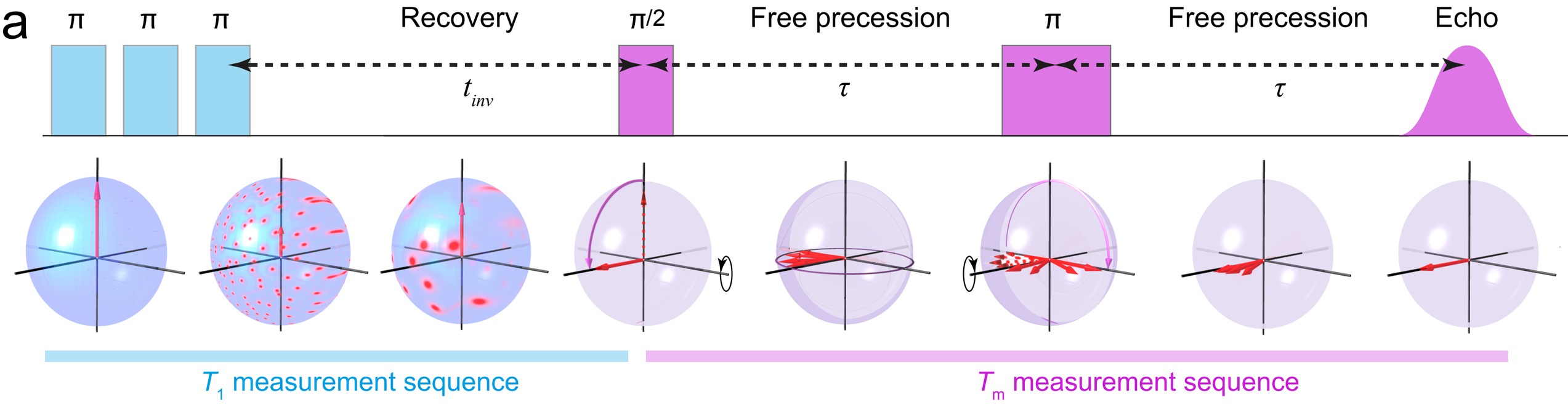
π
π
π
Recovery
π/2
Free precession
π
Free precession
Echo
t_{inv}
τ
τ
T_1 measurement sequence
T_m measurement sequence

b

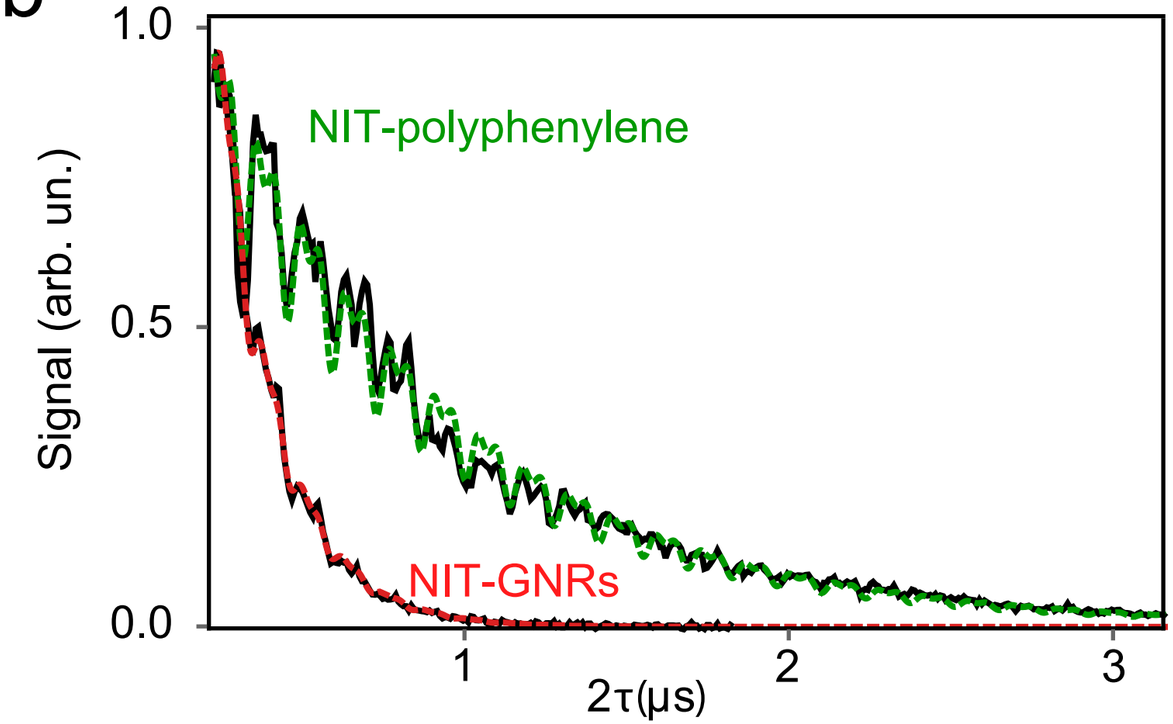
1.0
0.5
0.0
Signal (arb. un.)
NIT-polyphenylene
NIT-GNRs
1
2
3
2τ(μs)

c

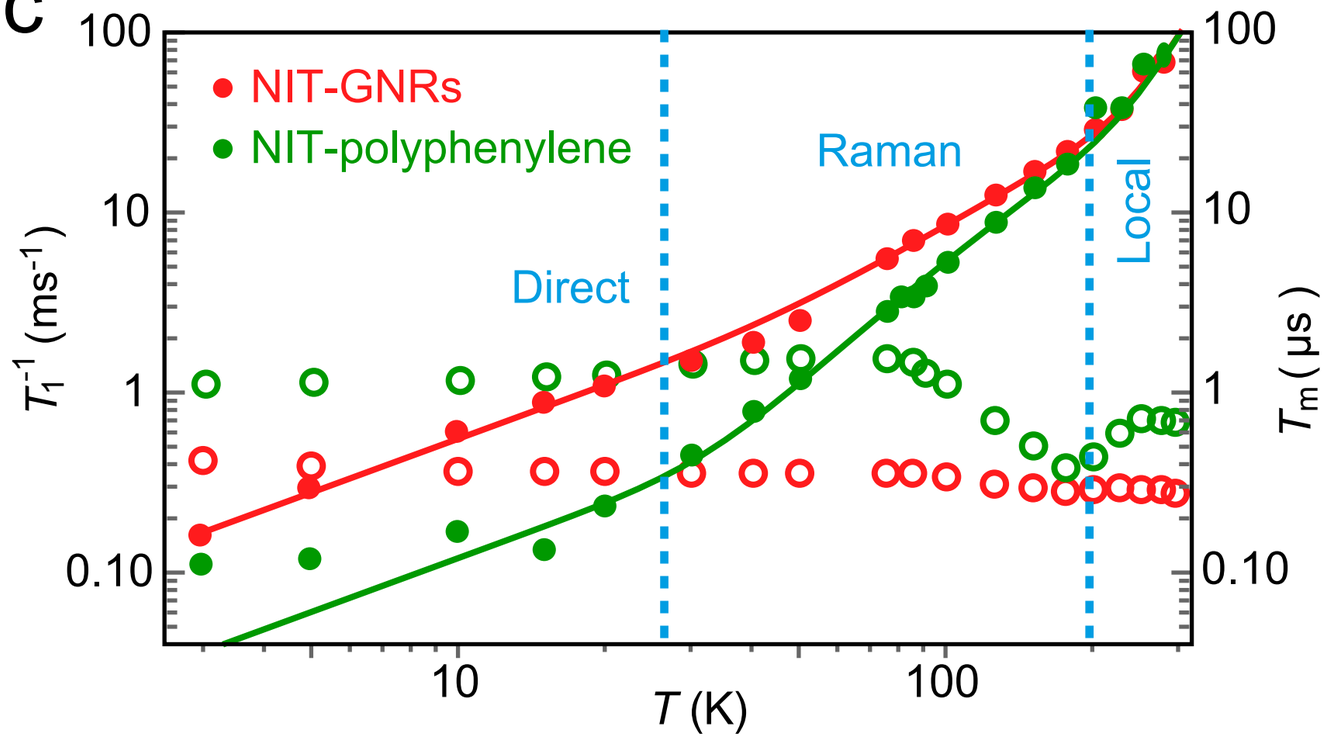
100
10
1
0.10
T_1^{-1} (ms^{-1})
NIT-GNRs
NIT-polyphenylene
Raman
Direct
Local
10
100
T (K)
T_m (μs)

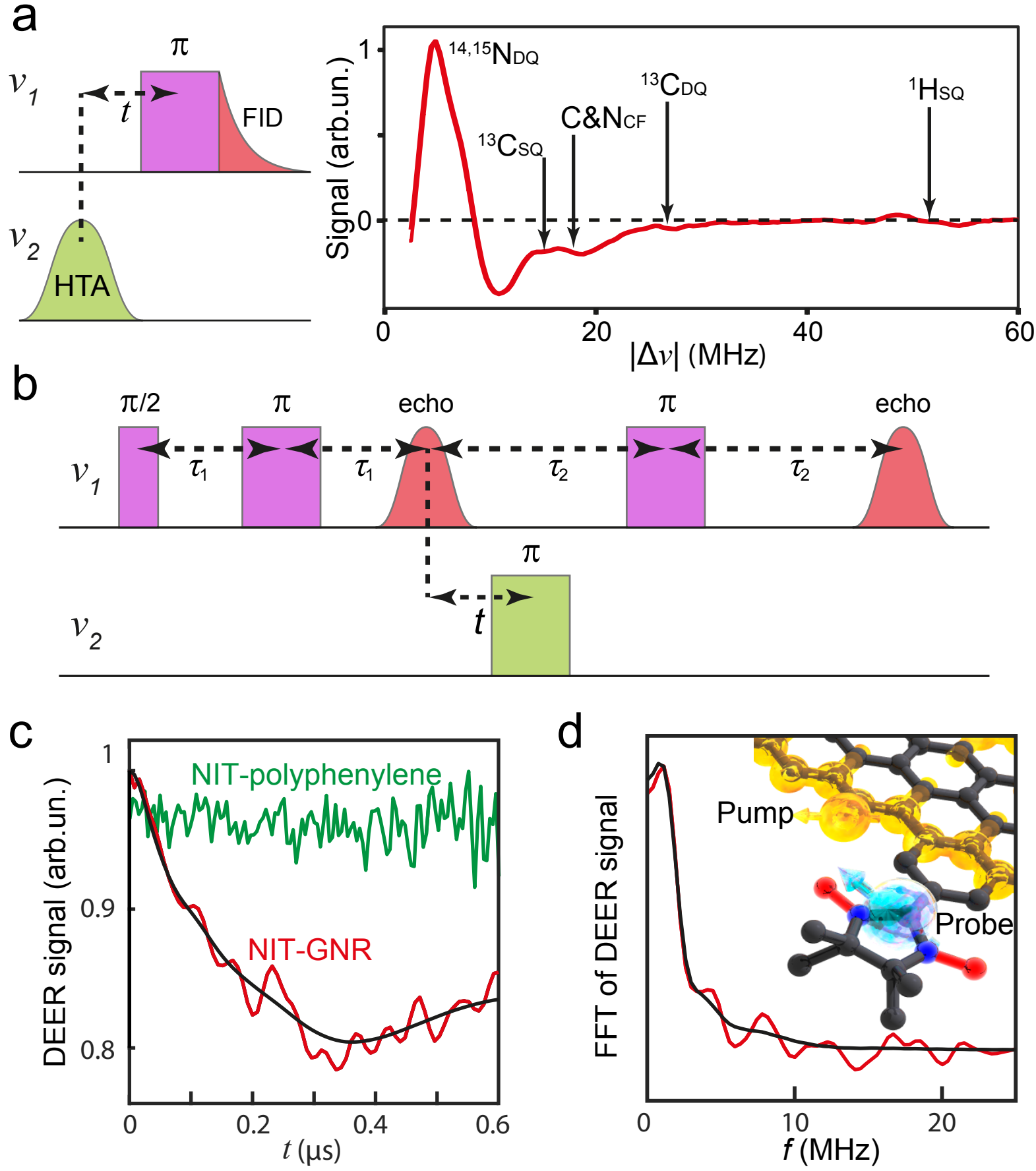
a
π
ν1
t
FID
ν2
HTA
Signal (arb.un.)
1
0
14,15NDQ
13CSQ
C&NCF
13CDQ
1HSQ
0
20
40
60
|Δν| (MHz)
b
π/2
π
echo
π
echo
ν1
τ1
τ1
τ2
τ2
π
t
ν2
c
DEER signal (arb.un.)
1
0.9
0.8
NIT-polyphenylene
NIT-GNR
0
0.2
0.4
0.6
t (μs)
d
FFT of DEER signal
Pump
Probe
0
10
20
f (MHz)